7. Maemondo M, Inoue A, Kobayashi K, *et al*: Gefitinib or chemotherapy for non-small-cell lung cancer with mutated EGFR. N Engl J Med 362: 2380-2388, 2010.
8. Zhou C, Wu YL, Chen G, *et al*: Erlotinib versus chemotherapy as first-line treatment for patients with advanced EGFR mutation-positive non-small-cell lung cancer (OPTIMAL, CTONG-0802): a multicentre, open-label, randomised, phase 3 study. Lancet Oncol 12: 735-742, 2011.
9. Rosell R, Carcereny E, Gervais R, *et al*: Erlotinib versus standard chemotherapy as first-line treatment for European patients with advanced EGFR mutation-positive non-small-cell lung cancer (EURTAC): a multicentre, open-label, randomised phase 3 trial. Lancet Oncol 13: 239-246, 2012.
10. Pao W, Miller VA, Politi KA, *et al*: Acquired resistance of lung adenocarcinomas to gefitinib or erlotinib is associated with a second mutation in the EGFR kinase domain. PLoS Med 2: e73, 2005.
11. Kobayashi S, Boggon TJ, Dayaram T, *et al*: EGFR mutation and resistance of non-small-cell lung cancer to gefitinib. N Engl J Med 352: 786-792, 2005.
12. Fujita Y, Suda K, Kimura H, *et al*: Highly sensitive detection of EGFR T790M mutation using colony hybridization predicts favorable prognosis of patients with lung cancer harboring activating EGFR mutation. J Thorac Oncol 7: 1640-1644, 2012.
13. Su KY, Chen HY, Li KC, *et al*: Pretreatment epidermal growth factor receptor (EGFR) T790M mutation predicts shorter EGFR tyrosine kinase inhibitor response duration in patients with non-small-cell lung cancer. J Clin Oncol 30: 433-440, 2012.
14. Rosell R, Molina MA, Costa C, *et al*: Pretreatment EGFR T790M mutation and BRCA1 mRNA expression in erlotinib-treated advanced non-small-cell lung cancer patients with EGFR mutations. Clin Cancer Res 17: 1160-1168, 2011.
15. Shepherd FA, Douillard JY and Blumenschein GR Jr: Immunotherapy for non-small cell lung cancer: novel approaches to improve patient outcome. J Thorac Oncol 6: 1763-1773, 2011.
16. Rosenberg SA, Yang JC and Restifo NP: Cancer immunotherapy: moving beyond current vaccines. Nat Med 10: 909-915, 2004.
17. Kawakami Y, Wang X, Shofuda T, *et al*: Isolation of a new melanoma antigen, MART-2, containing a mutated epitope recognized by autologous tumor-infiltrating T lymphocytes. J Immunol 166: 2871-2877, 2001.
18. Lennerz V, Fatho M, Gentilini C, *et al*: The response of autologous T cells to a human melanoma is dominated by mutated neoantigens. Proc Natl Acad Sci USA 102: 16013-16018, 2005.
19. Yoshikawa T, Nakatsugawa M, Suzuki S, *et al*: HLA-A2-restricted glypican-3 peptide-specific CTL clones induced by peptide vaccine show high avidity and antigen-specific killing activity against tumor cells. Cancer Sci 102: 918-925, 2011.
20. Valmori D, Fonteneau JF, Lizana CM, *et al*: Enhanced generation of specific tumor-reactive CTL in vitro by selected Melan-A/MART-1 immunodominant peptide analogues. J Immunol 160: 1750-1758, 1998.
21. Parkhurst MR, Salgaller ML, Southwood S, *et al*: Improved induction of melanoma-reactive CTL with peptides from the melanoma antigen gp100 modified at HLA-A*0201-binding residues. J Immunol 157: 2539-2548, 1996.
22. Fong L, Hou Y, Rivas A, *et al*: Altered peptide ligand vaccination with Flt3 ligand expanded dendritic cells for tumor immunotherapy. Proc Natl Acad Sci USA 98: 8809-8814, 2001.
23. Hirano N, Butler MO, Xia Z, *et al*: Engagement of CD83 ligand induces prolonged expansion of $CD8^+$ T cells and preferential enrichment for antigen specificity. Blood 107: 1528-1536, 2006.
24. Yoshimura M, Tada Y, Ofuzi K, Yamamoto M and Nakatsura T: Identification of a novel HLA-A*02:01-restricted cytotoxic T lymphocyte epitope derived from the EML4-ALK fusion gene. Oncol Rep 32: 33-39, 2014.
25. Rubio V, Stuge TB, Singh N *et al*: Ex vivo identification, isolation and analysis of tumor-cytolytic T cells. Nat Med 9: 1377-1382, 2003.
26. Warren RL and Holt RA: A census of predicted mutational epitopes suitable for immunologic cancer control. Hum Immunol 71: 245-254, 2010.
27. Soverini S, Hochhaus A, Nicolini FE, *et al*: BCR-ABL kinase domain mutation analysis in chronic myeloid leukemia patients treated with tyrosine kinase inhibitors: recommendations from an expert panel on behalf of European LeukemiaNet. Blood 118: 1208-1215, 2011.
28. Cai A, Keskin DB, DeLuca DS, *et al*: Mutated BCR-ABL generates immunogenic T-cell epitopes in CML patients. Clin Cancer Res 18: 5761-5772, 2012.
29. Yamshchikov GV, Barnd DL, Eastham S, *et al*: Evaluation of peptide vaccine immunogenicity in draining lymph nodes and peripheral blood of melanoma patients. Int J Cancer 92: 703-711, 2001.
30. Chen W, Yewdell JW, Levine RL and Bennink JR: Modification of cysteine residues in vitro and in vivo affects the immunogenicity and antigenicity of major histocompatibility complex class I-restricted viral determinants. J Exp Med 189: 1757-1764, 1999.
31. Meadows L, Wang W, den Haan JM, *et al*: The HLA-A*0201-restricted H-Y antigen contains a posttranslationally modified cysteine that significantly affects T cell recognition. Immunity 6: 273-281, 1997.
32. Shomura H, Shichijo S, Matsueda S, *et al*: Identification of epidermal growth factor receptor-derived peptides immunogenic for HLA-A2(+) cancer patients. Br J Cancer 90: 1563-1571, 2004.
33. Shomura H, Shichijo S, Komatsu N, *et al*: Identification of epidermal growth factor receptor-derived peptides recognised by both cellular and humoral immune responses in $HLA\text{-}A24^+$ non-small cell lung cancer patients. Eur J Cancer 40: 1776-1786, 2004.
34. Lu YC, Yao X, Li YF, *et al*: Mutated PPP1R3B is recognized by T cells used to treat a melanoma patient who experienced a durable complete tumor regression. J Immunol 190: 6034-6042, 2013.
35. Robbins PF, Lu YC, El-Gamil M, *et al*: Mining exomic sequencing data to identify mutated antigens recognized by adoptively transferred tumor-reactive T cells. Nat Med 19: 747-752, 2013.
36. Falk K, Rötzschke O, Stevanović S, Jung G and Rammensee HG: Allele-specific motifs revealed by sequencing of self-peptides eluted from MHC molecules. Nature 351: 290-296, 1991.
37. Sidney J, Southwood S, Mann DL, Fernandez-Vina MA, Newman MJ and Sette A: Majority of peptides binding HLA-A*0201 with high affinity crossreact with other A2-supertype molecules. Hum Immunol 62: 1200-1216, 2001.
38. Matsushita H, Vesely MD, Koboldt DC, *et al*: Cancer exome analysis reveals a T-cell-dependent mechanism of cancer immunoediting. Nature 482: 400-404, 2012.
39. Schirle M, Keilholz W, Weber B, *et al*: Identification of tumor-associated MHC class I ligands by a novel T cell-independent approach. Eur J Immunol 30: 2216-2225, 2000.
40. Parkhurst MR, Riley JP, Igarashi T, Li Y, Robbins PF and Rosenberg SA: Immunization of patients with the hTERT:540-548 peptide induces peptide-reactive T lymphocytes that do not recognize tumors endogenously expressing telomerase. Clin Cancer Res 10: 4688-4698, 2004.
41. Matar P, Alaniz L, Rozados V, *et al*: Immunotherapy for liver tumors: present status and future prospects. J Biomed Sci 16: 30, 2009.
42. Pollack BP, Sapkota B and Cartee TV: Epidermal growth factor receptor inhibition augments the expression of MHC class I and II genes. Clin Cancer Res 17: 4400-4413, 2011.
43. He S, Yin T, Li D, *et al*: Enhanced interaction between natural killer cells and lung cancer cells: involvement in gefitinib-mediated immunoregulation. J Transl Med 11: 186, 2013.
44. Yamada T, Azuma K, Muta E, *et al*: EGFR T790M mutation as a possible target for immunotherapy; identification of HLA-A*0201-restricted T cell epitopes derived from the EGFR T790M mutation. PLoS One 8: e78389, 2013.

HEPATOLOGY
Official Journal of the American Association for the Study of Liver Diseases

Gd-EOB-DTPA-Enhanced Magnetic Resonance Imaging and Alpha-Fetoprotein Predict Prognosis of Early-Stage Hepatocellular Carcinoma

Taro Yamashita,[1,2] Azusa Kitao,[3] Osamu Matsui,[3] Takehiro Hayashi,[2] Kouki Nio,[2] Mitsumasa Kondo,[2] Naoki Ohno,[4] Tosiaki Miyati,[4] Hikari Okada,[2] Tatsuya Yamashita,[2] Eishiro Mizukoshi,[2] Masao Honda,[2] Yasuni Nakanuma,[5] Hiroyuki Takamura,[6] Tetsuo Ohta,[6] Yasunari Nakamoto,[7] Masakazu Yamamoto,[8] Tadatoshi Takayama,[9] Shigeki Arii,[10] XinWei Wang,[11] and Shuichi Kaneko[2]

The survival of patients with hepatocellular carcinoma (HCC) is often individually different even after surgery for early-stage tumors. Gadolinium ethoxybenzyl diethylenetriamine pentaacetic acid (Gd-EOB-DTPA)-enhanced magnetic resonance imaging (MRI) has been introduced recently to evaluate hepatic lesions with regard to vascularity and the activity of the organic anion transporter OATP1B3. Here we report that Gd-EOB-DTPA-enhanced MRI (EOB-MRI) in combination with serum alpha-fetoprotein (AFP) status reflects the stem/maturational status of HCC with distinct biology and prognostic information. Gd-EOB-DTPA uptake in the hepatobiliary phase was observed in ~15% of HCCs. This uptake correlated with low serum AFP levels, maintenance of hepatocyte function with the up-regulation of *OATP1B3* and *HNF4A* expression, and good prognosis. By contrast, HCC showing reduced Gd-EOB-DTPA uptake with high serum AFP levels was associated with poor prognosis and the activation of the oncogene *FOXM1*. Knockdown of *HNF4A* in HCC cells showing Gd-EOB-DTPA uptake resulted in the increased expression of *AFP* and *FOXM1* and the loss of *OATP1B3* expression accompanied by morphological changes, enhanced tumorigenesis, and loss of Gd-EOB-DTPA uptake *in vivo*. HCC classification based on EOB-MRI and serum AFP levels predicted overall survival in a single-institution cohort (n = 70), and its prognostic utility was validated independently in a multi-institution cohort of early-stage HCCs (n = 109). *Conclusion*: This noninvasive classification system is molecularly based on the stem/maturation status of HCCs and can be incorporated into current staging practices to improve management algorithms, especially in the early stage of disease. (HEPATOLOGY 2014;60:1674-1685)

Liver cancer is the fifth most commonly diagnosed cancer and the second most frequent cause of cancer death in men worldwide.[1] Among primary liver cancers, hepatocellular carcinoma (HCC) represents the major histological subtype, accounting for 70-86% of cases of primary liver cancer.[1] Several staging systems are currently available for HCC classification and include Tumor Node

Abbreviations: AFP, alpha-fetoprotein; BCLC, Barcelona Clinic Liver Cancer; EOB-MRI, gadolinium ethoxybenzyl diethylenetriamine pentaacetic acid-enhanced magnetic resonance imaging; FOXM1, forkhead box protein M1; Gd-EOB-DTPA, gadolinium ethoxybenzyl diethylenetriamine pentaacetic acid; HCC, hepatocellular carcinoma; HNF4α, hepatocyte nuclear factor 4 alpha; IHC, immunohistochemistry; MRI, magnetic resonance imaging; NOD/SCID, nonobese diabetic, severe combined immunodeficient; OATPs, organic anion transporting polypeptides; qRT-PCR, quantitative reverse-transcription polymerase chain reaction; SI, signal intensity; TNM, tumor node metastasis.

From the [1]Department of General Medicine, Kanazawa University Graduate School of Medical Science, Kanazawa, Ishikawa, Japan; [2]Department of Gastroenterology, Kanazawa University Graduate School of Medical Science, Kanazawa, Ishikawa, Japan; [3]Department of Radiology, Kanazawa University Graduate School of Medical Science, Kanazawa, Ishikawa, Japan; [4]Faculty of Health Sciences, Institute of Medical, Pharmaceutical and Health Sciences, Kanazawa University, Kanazawa, Ishikawa, Japan; [5]Department of Pathology, Kanazawa University Graduate School of Medical Science, Kanazawa, Ishikawa, Japan; [6]Department of Gastroenterologic Surgery, Kanazawa University Graduate School of Medical Science, Kanazawa, Ishikawa, Japan; [7]Second Department of Internal Medicine, Fukui University School of Medicine, Fukui, Japan; [8]Department of Surgery, Institute of Gastroenterology, Tokyo Women's Medical University, Tokyo, Japan; [9]Department of Digestive Surgery, Nihon University School of Medicine, Tokyo, Japan; [10]Department of Hepato-Biliary-Pancreatic Surgery, Tokyo Medical and Dental University, Tokyo, Japan; [11]Laboratory of Human Carcinogenesis, Center for Cancer Research, National Cancer Institute, Bethesda, MD, USA.

Received September 19, 2013; accepted February 20, 2014.

Metastasis (TNM) and Barcelona Clinic Liver Cancer (BCLC) staging, which are based on tumor number and size, vascular invasion, metastatic status, hepatic reserve, and performance status.[2] These systems can provide an approximate estimate of patients' survival, but patients diagnosed at the same disease stage sometimes show a different prognosis. This is most likely because these systems do not include an assessment of the malignant phenotype of the tumor, which would be especially important in those patients diagnosed at the early stage of disease. To overcome these limitations, gene expression profiling technologies have been applied to classify HCC. In particular, the stemness of HCC is currently of great interest because its gene expression profile reflects the malignant nature of the tumor.[3-7] However, the application of these new technologies still needs to be validated externally prior to their implementation in clinical practice.

The hallmark of HCC diagnosis has been image analysis based on vascularity. Gadolinium ethoxybenzyl diethylenetriamine pentaacetic acid (Gd-EOB-DTPA) is a liver-specific magnetic resonance imaging (MRI) contrast agent introduced specifically to improve the detection of liver lesions.[8] Gd-EOB-DTPA-enhanced MRI (EOB-MRI) has been used to evaluate liver tumors in Europe since 2004, in the USA and Japan since 2008, and in China since 2010. Gd-EOB-DTPA is characterized by its rapid and specific uptake by hepatocytes by way of organic anion transporting polypeptides (OATPs) expressed in the sinusoidal membrane. Therefore, Gd-EOB-DTPA uptake in the liver is considered to reflect hepatocyte function.[9] Among OATP1A2, 1B1, 1B3, and 2B1, only OATP1B3 expression was found to correlate with the enhancement ratio on EOB-MRI, indicating that it transports Gd-EOB-DTPA into HCC cells.[10] It is generally accepted that ~85% of HCCs show hypointensity in the hepatobiliary phase of EOB-MRI compared to the noncancerous background liver, with a reduction of OATP1B3 protein or *OATP1B3* gene expression in the tumor.[10,11] However, atypical Gd-EOB-DTPA uptake in the hepatobiliary phase is observed in the remaining 15% of HCCs, and the molecular phenotype and clinical features of these HCCs remain to be elucidated.

We hypothesized that EOB-MRI findings may vary in different tumor subtypes with distinct biology. Therefore, in this study we evaluated the molecular profiles of HCCs in a single-institute cohort determined from the EOB-MRI findings using quantitative reverse-transcription polymerase chain reaction (qRT-PCR), microarray, and immunohistochemistry (IHC) analyses. To clarify the clinical utility of the EOB-MRI findings, we also evaluated the prognosis of a multicenter cohort of patients with early-stage HCC who underwent radical resection.

Materials and Methods

Patients. A total of 417 patients who received surgical resection for HCC were enrolled in this study. Seventy patients underwent EOB-MRI for the diagnosis of HCC and received surgical resection at Kanazawa University Hospital from 2008 to 2011. Survival analysis was performed in this single-institute cohort (Cohort 1) and prognosis was evaluated every 6 months. The final evaluation of survival was performed in October 2011. From these 70 patients, 62 tumor and nontumor samples were snap-frozen in liquid nitrogen and used for qRT-PCR.

For microarray analysis, we assessed 238 patients who received surgical resection of HCC at the Liver Cancer Institute of Fudan University. EOB-MRI was not performed in these patients because Gd-EOB-DTPA had not yet been introduced in China. Their clinicopathologic characteristics and prognostic data have been described previously.[12]

To evaluate the survival of early-stage HCCs, we enrolled 109 patients who received EOB-MRI and surgical resection at Tokyo Medical and Dental University Hospital, Tokyo Women's Medical University Hospital, Nihon University School of Medicine Itabashi Hospital, Niigata University Medical & Dental Hospital, Hyogo College of Medicine Hospital, or Kurume

Supported by Health and Labor Sciences Research Grants for "Development of novel molecular markers and imaging modalities for earlier diagnosis of hepatocellular carcinoma," Grants from the Ministry of Education, Culture, Sports, Science, and Technology of Japan, the National Cancer Center Research and Development Fund (23-B-5), and the Intramural Research Program Grant (Z01 BC 010313) of the Center for Cancer Research, US National Cancer Institute.

Address reprint requests to: Taro Yamashita, M.D., Ph.D., Assistant Professor, Department of Gastroenterology/General Medicine, Kanazawa University Graduate School of Medical Science, 13-1 Takara-Machi, Kanazawa, Ishikawa 920-8641, Japan. E-mail: taroy@m-kanazawa.jp; fax: +81-76-234-4250.

View this article online at wileyonlinelibrary.com.

DOI 10.1002/hep.27093

Potential conflict of interest: Dr. Matsui is on the speakers' bureau for Bayer.

University Hospital from 2008 to 2009 (Cohort 2). The prognosis of these patients was evaluated every year, and the final evaluation of survival was performed in February 2012.

This study was approved by the Institutional Review Board at each study center and all patients provided written informed consent.

EOB-MRI. EOB-MRI was performed before surgical resection using a 1.5 or 3.0 Tesla MRI system with a fat-suppressed 2D or 3D gradient echo T1-weighted sequence (relaxation time / echo time [TR/TE] = 3.2-3.6/1.6-2.3 ms, flip angle 10-15°, field of view 33-42 cm, matrix 128-192 × 256-512, slice thickness 4.0-8.0 mm). A dose of 0.025 mmol/kg Gd-EOB-DTPA (Primovist; Bayer Schering Pharma, Berlin, Germany) was injected intravenously and the hepatobiliary phase was obtained at 15-20 minutes after the injection.

All abdominal MRI data of the HCC patients were generated at Kanazawa University Hospital and image analysis was performed retrospectively by two radiologists (A.K. and O.M.) without knowledge of the clinical and pathological results. The signal intensity (SI) of the tumor was measured within the region of interest, which was determined as the maximum oval area at the largest section of the tumor. The SI of the adjacent background liver was also measured within a region of interest of the same size, while avoiding large vessels. The nodules were classified into the two following types: hypointense HCC, which was defined as showing a lower SI than that of the surrounding liver (tumor SI / background SI <1.0) in the hepatobiliary phase, and hyperintense HCC, which was defined as showing an equal or higher SI (tumor SI / background SI ≥ 1.0).

For the mouse study, EOB-MRI was performed using a 0.4 T MRI system with a fat-suppressed 3D gradient echo T1-weighted sequence (TR/TE = 66.5/4.0 ms, flip angle 40°, field of view 10 cm, matrix 224 × 192, slice thickness 1.0 mm). A dose of 0.025 mmol/kg Gd-EOB-DTPA (Bayer Schering Pharma) was injected through the tail vein, and the hepatobiliary phase was obtained at 12-20 minutes after the injection.

Xenotransplantation of Primary HCC in Immunodeficient Mice and* HNF4A *Knockdown. Primary HCC tissue was dissected and digested in 1 mg/mL type 4 collagenase solution (Sigma-Aldrich Japan, Tokyo, Japan) at 37°C for 15-30 minutes. Contaminated red blood cells were lysed with an ammonium chloride solution (STEMCELL Technologies, Vancouver, BC, Canada) on ice for 5 minutes. $CD45^+$ leukocytes and annexin V^+ apoptotic cells were removed by an autoMACS-pro cell separator and magnetic beads (Miltenyi Biotec, Tokyo, Japan). The cells were suspended 1:1 in 200 μL Dulbecco's modified Eagle's medium (DMEM) and Matrigel (BD Biosciences) and injected subcutaneously into 6-week-old NOD/SCID mice (NOD/NCrCRl-*Prkdc*^{scid}) purchased from Charles River Laboratories (Wilmington, MA). EOB-MRI was performed to evaluate Gd-EOB-DTPA uptake in the subcutaneous tumor at the hepatobiliary phase, and the subcutaneous tumor was dissected and digested as described above, and subsequently cultured in DMEM. *HNF4A* knockdown was performed using pGFP-V-RS vectors (OriGene Technologies, Rockville, MD), allowing stable delivery of the short hairpin RNA (shRNA) expression cassette against *HNF4A* or scramble sequence into host cells by way of a replication-deficient retrovirus. Infected HCC cells were grown in DMEM containing 1 μg/mL puromycin (Sigma-Aldrich Japan) for 7 days to establish stable shRNA-expressing HCC cells. Western blotting and immunofluorescence analyses were performed using an antihuman HNF4α C11F12 antibody (Cell Signaling Technology, Danvers, MA) and a mouse monoclonal antihuman OATP1B3 MDQ/5F260 antibody (Novus Biologicals, Littleton, CO), essentially as described previously.[13] Control or Sh-HNF4A-transfected HCC cells were injected subcutaneously into NOD/SCID mice, and tumor volume and survival were evaluated every 2-3 days. The protocol was approved by the Kanazawa University Animal Care and Use Committee and the Kanazawa University Genetic Modification Experiment Committee.

Microarray Analysis. The 238 HCC cases from the Liver Cancer Institute of Fudan University with available microarray data and clinicopathologic and prognostic data have been described previously.[12] BRB-ArrayTools software (v. 3.8.1) was used for class comparison analysis. Hierarchical clustering analysis was performed with Genesis software (v. 1.6.0 beta). Canonical pathway and transcription factor analyses were performed using MetaCore software (http://www.genego.com). Interaction network analysis was performed using Ingenuity Pathway Analysis software (http://www.ingenuity.com).

qRT-PCR Analysis. Total RNA was extracted using an RNeasy Mini Kit (Qiagen, Valencia, CA) according to the manufacturer's instructions. The expression of selected genes was determined in triplicate using the Applied Biosystems 7900HT Sequence Detection System (Applied Biosystems, Foster City, CA) and the $-\Delta\Delta$CT method. The following probes were used: *AFP*, Hs00173490_m1; *FOXM1*, Hs01073586_m1; *OATP1B3*, Hs00251986_m1; *CYP3A4*, Hs00430021_m1; and *18S*, Hs99999901_s1 (Applied Biosystems).

IHC Analysis. IHC was performed using Envision+ kits (Dako Japan, Tokyo, Japan) as described previously.[14] Mouse monoclonal antihuman Ki-67 antigen MIB-1 (Dako Japan), mouse monoclonal antihuman OATP1B3 MDQ/5F260 (Novus Biologicals), rabbit monoclonal antihuman HNF4α C11F12 (Cell Signaling Technology), mouse monoclonal antihuman FOXM1 0.T.181 (Abcam, Cambridge, MA), mouse monoclonal antihuman glypican-3 1G12 (BioMosaics, Burlington, VT), and mouse monoclonal antiglutamine synthetase clone GS-6 (Millipore, Billerica, MA) antibodies were used. The staining area and intensities were evaluated in each sample and graded from 0-3 (0, 0-5%; 1, 5-25%; 2, 25-50%; 3, >50%) and 0-2 (0, negative; 1, weak; 2, strong), respectively. The sum of the area and intensity scores of each marker (IHC score) were calculated. Samples were defined as marker-high (IHC score ≥3) or -low (IHC score ≤2). The Ki-67 labeling index was calculated as described previously.[14]

Statistical Analysis. Mann-Whitney, χ^2, Fisher's exact, and Kruskal-Wallis tests were used to compare the clinicopathologic characteristics and gene expression data. The correlation of the gene expression data was evaluated by Spearman's rank correlation coefficient. Kaplan-Meier survival analysis with the log-rank test was performed to compare patient survival. All analyses were performed using GraphPad Prism software v. 5.0.1 (GraphPad Software, San Diego, CA).

Results

EOB-MRI Findings and Molecular Characteristics of HCC. Nine of the 70 HCC cases (12.9%) in Cohort 1 were diagnosed with hyperintense HCC on EOB-MRI (Fig. 1A). Analysis of the clinicopathologic characteristics of hyper- or hypointense HCCs revealed that hyperintense HCCs were significantly associated with low serum alpha-fetoprotein (AFP) levels (Table 1). There was no significant difference between hyper- and hypointense HCCs in terms of other factors, including tumor size, number, TNM and BCLC stages, surgical procedures, and elapsed time between MRI and surgery. We confirmed the overexpression of OATP1B3, a transporter responsible for the uptake of Gd-EOB-DTPA in hepatocytes, in hyperintense HCCs by qRT-PCR and IHC (Fig. 1B).

To understand the transcriptomic characteristics of HCCs overexpressing *OATP1B3*, we analyzed the microarray data of an additional 238 HCC cases.[12] *OATP1B3*-high and -low HCCs were defined as HCCs with a T/N ratio ≥1.0 and <1.0, respectively, as used for the evaluation of hyperintense HCCs (tumor SI / background SI ≥1.0). The frequency of *OATP1B3*-high HCCs was 15.1% (36 of the 238 HCC cases), almost comparable to the frequency of hyperintense HCCs reported thus far. Class-comparison analysis yielded a total of 974 genes that were differentially expressed between *OATP1B3*-high and -low HCCs ($P < 0.001$). Hierarchical cluster analysis of this 974 gene set (*OATP1B3* gene signature) separated HCCs into two branches (B1 and B2) (Fig. 1C). Thirty-four of the 36 *OATP1B3*-high HCCs (blue box) were classified in the left branch (B1), while *OATP1B3*-low HCCs were clustered in both branches. The prognosis of HCC patients clustered in B1 was significantly better than those clustered in B2 ($P = 0.02$) (Supporting Fig. S1). Genes associated with mature hepatocyte function such as *ALB* and *CYP3A4* were significantly up-regulated in the HCCs clustered in B1, and the known hepatic stem/progenitor markers *KRT19* and *EPCAM*, as well as the G1/S cell cycle marker *MKI67*, were significantly up-regulated in the HCCs clustered in B2 (Fig. 1D).

Pathway analysis indicated that *OATP1B3*-high HCCs showed maintenance of mature hepatocyte function and decreased cell proliferation and Wnt signaling (Fig. 1E), which are known to be activated during liver development and regeneration.[15] Transcription factor analysis identified eight genes (*HNF4A, NFIA, NR3C1, NR1I3, ESR1, NR1H3, MLXIPL*, and *NFE2L2*) as candidate transcription factors that were significantly activated in *OATP1B3*-high HCCs ($P < 0.005$) (Fig. 1F). These transcription factors are known to play a pivotal role in liver development and in the regulation of hepatocyte functions including lipid, bile, carbohydrate, and xenobiotic metabolism.[16] By contrast, only one gene (*FOXM1*) was identified as a candidate transcription factor activated in *OATP1B3*-low HCCs. The forkhead box M1 (FOXM1) transcription factor is known to be activated during liver regeneration and regulation of the cell cycle.[17] We investigated the expression of the two transcription factors most strongly activated (*HNF4A* encoding hepatocyte nuclear factor 4 alpha [HNF4α]) or inactivated (*FOXM1*) in hyperintense HCCs (Fig. S2) and validated the results using microarray analyses (Fig. 2A,B).

Although the microarray data revealed distinct molecular portraits associated with liver development and the maturation programs present in hyper- and hypointense HCCs, hierarchical cluster analysis further indicated that a subset of hypointense HCCs (corresponding to the *OATP1B3*-low HCCs clustered in B1)

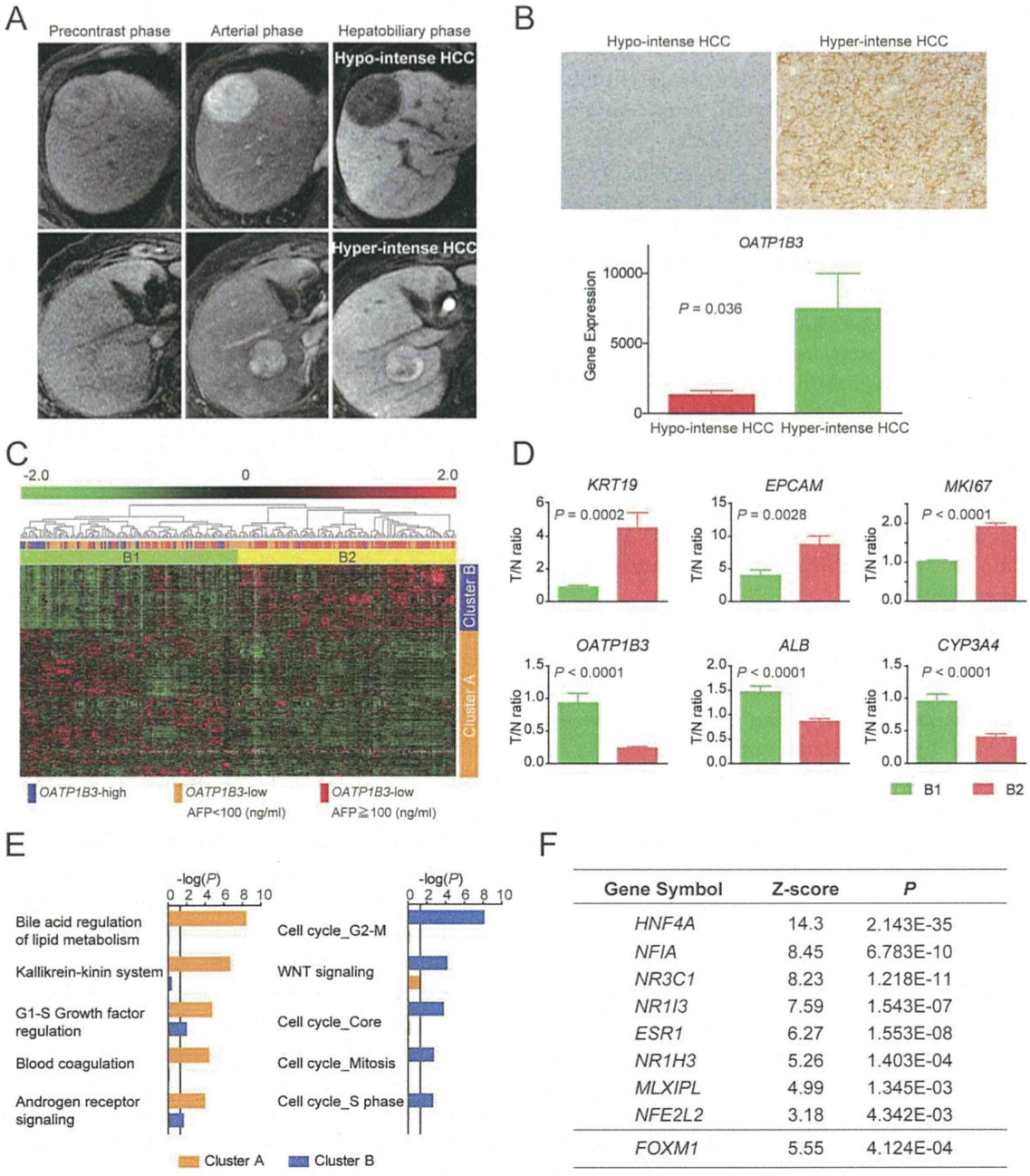

F

Gene Symbol	Z-score	P
HNF4A	14.3	2.143E-35
NFIA	8.45	6.783E-10
NR3C1	8.23	1.218E-11
NR1I3	7.59	1.543E-07
ESR1	6.27	1.553E-08
NR1H3	5.26	1.403E-04
MLXIPL	4.99	1.345E-03
NFE2L2	3.18	4.342E-03
FOXM1	5.55	4.124E-04

Fig. 1. Molecular profiles of HCCs corresponding to the EOB-MRI findings. (A) Representative MRI scans of hypo- and hyperintense HCCs in the precontrast, arterial, and hepatobiliary phases. The T/N signal intensity ratios of the images in the hepatobiliary phase were 0.47 (upper panel) and 1.07 (lower panel). (B) Upper panel: Representative photomicrographs of IHC staining with an anti-OATP1B3 antibody in hypo- and hyperintense HCCs. Lower panel: *OATP1B3* expression in hypo- and hyperintense HCCs. (C) The expression patterns of *OATP1B3* signatures in *OATP1B3*-high (blue box), *OATP1B3*-low AFP-low (<100 ng/mL) (orange box), and *OATP1B3*-low AFP-high (≥100 ng/mL; red box) after hierarchical clustering of genes and samples, shown as a heat map image. Red indicates a high expression level; green indicates a low expression level. *OATP1B3*-high HCCs and *OATP1B3*-low AFP-high HCCs were clustered in B1 (green bar) and B2 (yellow bar), respectively. (D) Representative expression of genes in clusters A (*KRT19, EPCAM*, and *MKI67*) and B (*OATP1B3, ALB*, and *CYP3A4*). The green and orange bars indicate HCCs clustered in B1 and B2, respectively. (E) The activated pathways are identified in clusters A (orange bar) and B (blue bar). (F) Genes encoding transcription factors activated or inactivated in *OATP1B3*-high HCCs.

might show similar gene expression profiles to those observed in hyperintense HCCs. Since serum AFP levels are reportedly related to the stem/maturation subtypes of HCCs with different gene expression profiles,[12] we analyzed the characteristics of *OATP1B3*-low HCCs in 238 cases according to serum AFP levels. Interestingly, *OATP1B3*-low HCCs assigned to the left branch (B1) had low serum AFP

Table 1. Characteristics of HCCs Classified by EOB-MRI in Cohorts 1 and 2

	Cohort 1			Cohort 2		
Characteristics	Hyperintense (n = 9)	Hypointense (n = 61)	P*	Hyperintense (n = 9)	Hypointense (n = 100)	P*
Age (years, mean ± SE)	66.2 ± 3.6	64.6 ± 1.2	0.21	67.2 ± 2.0	66.2 ± 1.0	1.0
Sex (male/female)	7/2	44/17	0.72	9/0	79/21	0.13
Etiology (HBV/HCV/other)	2/3/4	14/23/24	0.95	1/6/0/2	22/56/2/20	0.52
Liver cirrhosis (yes/no)	5/4	33/28	0.94	2/7	42/58	0.25
AFP (ng/mL, mean ± SE)	12.4 ± 1.9	2,157 ± 866	0.03	7.0 ± 2.2	188.4 ± 74	0.03
Histologic grade†						
I–II	1	12		2	16	
II–III	8	38		7	74	
III–IV	0	11	0.25	0	10	0.57
Tumor size (cm, mean ± SE)	4.0 ± 0.9	4.4 ± 0.4	0.79	3.3 ± 0.4	2.6 ± 0.1	0.09
Tumor number (single/multiple)	7/2	48/13	0.95	8/1	86/14	0.81
Macroscopic portal vein invasion (yes/no)	1/8	5/56	0.58	0/9	0/100	
Microscopic portal vein invasion (yes/no)	2/7	27/34	0.21	0/9	11/89	0.59
Tumor-node-metastasis classification (I/II/III)	6/2/1	29/28/4	0.40	7/2/0	75/25/0	0.85
BCLC stage (0/A/B/C)	0/7/1/1	4/30/22/5	0.34	0/9/0/0	27/73/0/0	0.07
Elapsed time between MRI and surgery (days, mean ± SE)	47.0 ± 8.4	51.5 ± 3.2	0.73	17.3 ± 5.0	20.6 ± 3.0	0.50
Surgical procedure (partial resection or segmentectomy/ lobectomy or extended lobectomy)	6/3	35/26	0.60	8/1	86/14	1.0

*Mann–Whitney test, Fisher's exact test, or χ^2 test.
†Edmondson–Steiner.

levels (<100 ng/mL: orange box, Fig. 1C), while the majority of AFP-high (≥100 ng/mL) HCCs (red box, Fig. 1C) were clustered in the right branch (B2). Consistently, the *OATP1B3* gene signature significantly predicted the serum AFP status of 238 HCCs ($P < 0.05$) (Tables S1-3).

OATP1B3 and AFP Expression in HCC Subtypes Related to Stem/Maturational Status. Molecular profiling of tissue samples may be useful for predicting the survival of HCC patients, as reported previously.[18,19] However, such an approach should be established before being applied routinely in a clinical setting. The above data prompted us to hypothesize that EOB-MRI findings and serum AFP levels, in place of molecular profiling techniques, have the potential to categorize HCCs (EOB-AFP classification), thus serving as predictors of survival. We categorized HCCs into three groups (class A: hyperintense HCC, class B: hypointense and AFP-low [<100 ng/mL] HCC, and class C: hypointense and AFP-high [≥100 ng/mL] HCC). The clinicopathologic characteristics of patients with class A, B, and C HCCs in Cohort 1 are shown in Table S4.

We investigated the expression of HNF4α and FOXM1 as well as the G1/S marker Ki-67 by IHC according to the EOB-AFP classification system in Cohort 1 (Fig. 2C). HNF4α was most abundantly expressed in class A HCCs, but its expression was decreased in class B and C HCCs. By contrast, the expression of FOXM1 and Ki-67 was highest in class C HCCs, significantly decreased in class B HCCs, and not detected in class A HCCs. The mean Ki-67 labeling indices in class A, B, and C HCCs were 2.8%, 9.4%, and 18.2%, respectively ($P < 0.0001$) (Fig. 2D). The differences in FOXM1 and HNF4α expression among class A, B, and C HCCs were statistically significant (Fig. 2E).

We further investigated the expression of five markers (glypican 3, GPC-3; lymphatic vessel endothelial hyaluronan receptor 1, LYVE-1; survivin; heat shock 70 kDa protein, HSP70; and glutamine synthetase, GS), known to be differentially expressed between dysplastic nodule and well-differentiated HCC,[20,21] to clarify if the molecular alterations in early-stage hepatocarcinogenesis can be detected differentially in EOB-AFP class A, B, and C HCCs. IHC analysis suggested no differential expression of LYVE-1, survivin, and HSP70 among the EOB-AFP classes (data not shown). Interestingly, GS was most abundantly expressed in class A HCCs, and its expression was relatively decreased in class B and C HCCs with borderline significance ($P = 0.06$) (Fig. S3A,B). In contrast, GPC-3 expression was highest in class C HCCs and relatively decreased in class A and B HCCs with statistical significance ($P = 0.03$). We investigated the microarray data of 238 independent HCC cases and validated the positive correlation between *OATP1B3* and *GLUL* (encoding GS) and the weak negative correlation between *OATP1B3* and *GPC3* (encoding GPC-3).

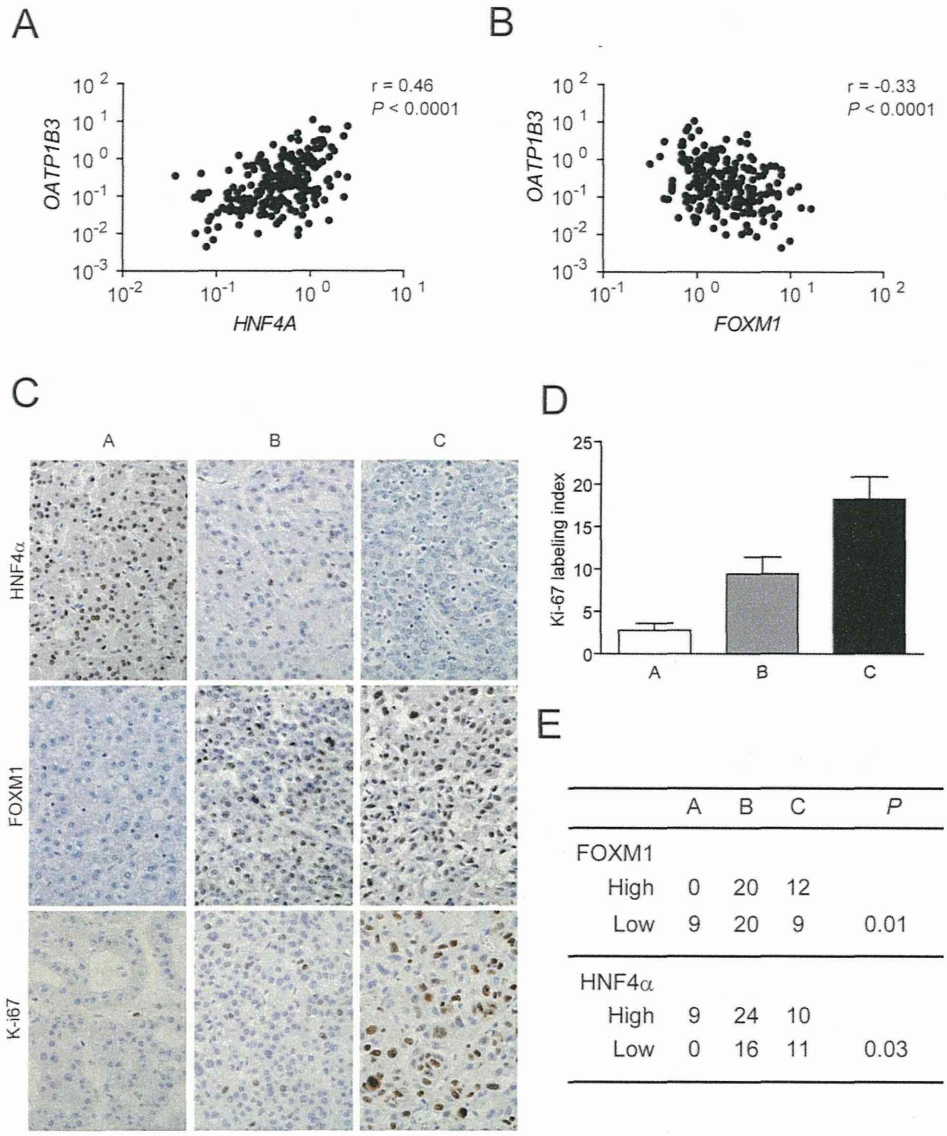

Fig. 2. Transcriptional programs of HCCs corresponding to the EOB-MRI findings and serum AFP. (A,B) Scatterplot analyses of the microarray data of 238 HCCs. (C) Representative photomicrographs of IHC staining with anti-HNF4α, anti-FOXM1, and anti-Ki-67 antibodies in class A, B, and C HCCs, according to the EOB-AFP classification. (D) Ki-67 labeling index in class A, B, and C HCCs. (E) Summary of FOXM1 and HNF4α expression in class A, B, and C HCCs.

Regulation of Gd-EOB-DTPA Uptake and Tumorigenic Capacity by HNF4α in Hyperintense HCC. Microarray and IHC analyses suggested the activation of transcription factor HNF4α in hyperintense HCC, but its role in the maintenance of hepatocyte function and Gd-EOB-DTPA uptake has not yet been clarified. To directly explore the role of HNF4α in Gd-EOB-DTPA uptake and tumorigenic capacities, we transplanted tumor cells from hyper- and hypointense primary HCC specimens into NOD/SCID mice (Fig. 3A). We confirmed on EOB-MRI that Gd-EOB-DTPA uptake capacity was relatively maintained in the secondary xenotransplanted tumors that developed in the subcutaneous lesions of the mice (Fig. 3B).

Using a retrovirus system *in vitro*, we then introduced shRNA targeting *HNF4A* (Sh-HNF4A) or scramble (Sh-Scr) into tumor cells obtained from a hyperintense HCC. We confirmed the reduction of HNF4α protein expression in Sh-HNF4A-transfected cells compared with Sh-Scr-transfected cells by western blotting (Fig. 3C, left panel). Interestingly, *HNF4A* knockdown resulted in a modest increase in *AFP* and *FOXM1* expression and a dramatic decrease in *CYP3A4* and *OATP1B3* expression (Fig. 3C, right panel). It also resulted in the loss of OATP1B3 protein expression, and striking morphological changes were confirmed by immunofluorescence and phase-contrast microscopy (Fig. 3D). Sh-HNF4A-transfected cells displayed long, thin cell shapes with neurite-like extensions, whereas Sh-Scr-transfected cells were relatively smooth and round. Sh-Scr- or Sh-HNF4A-transfected cells were further injected subcutaneously into NOD/SCID mice, and aggressive tumor growth accompanied with the loss of Gd-EOB-DTPA uptake capacity was

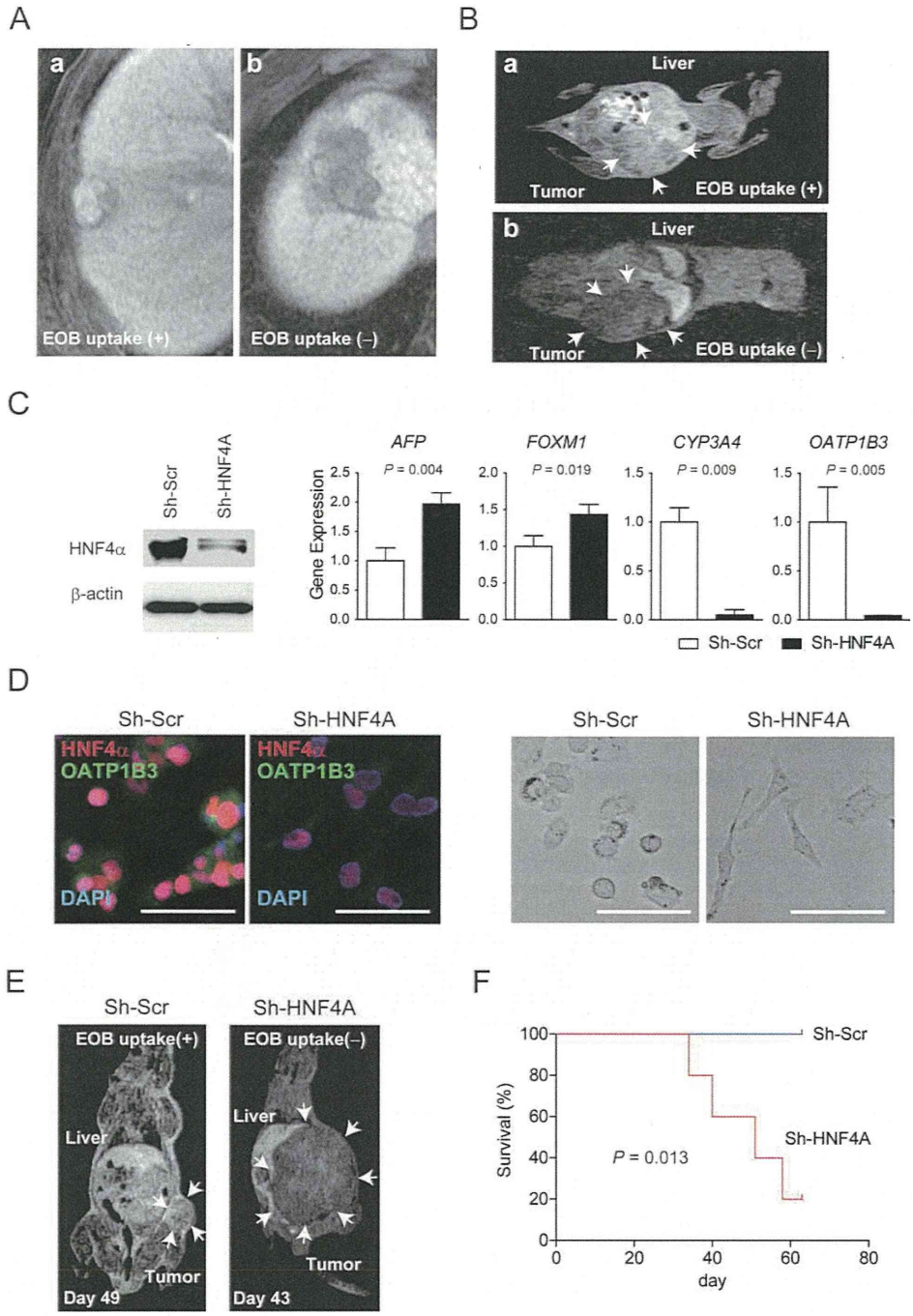

Fig. 3. HNF4α regulates a mature hepatocyte-like, less aggressive HCC phenotype coupled with Gd-EOB-DTPA uptake in hyperintense HCC. (A) MRI scans of hyperintense (a) and hypointense (b) HCCs in the hepatobiliary phase before surgery. The T/N signal intensity ratios of the images in the hepatobiliary phase were 1.02 (left panel) and 0.49 (right panel). Surgically resected specimens were subsequently used for mouse xenotransplantation. (B) MRI scans of NOD/SCID mouse xenotransplanted with hyperintense (a) and hypointense (b) HCCs in the hepatobiliary phase. The T/N signal intensity ratios of the images were 0.82 (upper panel) and 0.45 (lower panel). (C) Left panel: Expression of HNF4α protein by western blotting. Hyperintense HCC cells were harvested in dishes and treated with retroviruses encoding an expression cassette against *HNF4A* (Sh-HNF4A) or scramble sequence (Sh-Scr). Right panel: qRT-PCR of *AFP, FOXM1, CYP3A4*, and *OATP1B3* in hyperintense HCC cells transfected with Sh-Scr or Sh-HNF4A. (D) Left panel: Immunofluorescence analysis of HNF4α (red) and OATP1B3 (green) in hyperintense HCC cells transfected with Sh-Scr or Sh-HNF4A (scale bar = 100 μm). Right panel: Representative photomicrographs of hyperintense HCC cells transfected with Sh-Scr or Sh-HNF4A (scale bar = 100 μm). (E) MRI scans of NOD/SCID mouse xenotransplanted with hyperintense HCC cells transfected with Sh-Scr (day 49 after transplantation) or Sh-HNF4A (day 43 after transplantation). The T/N signal intensity ratios of the images in the hepatobiliary phase were 0.65 (left panel) and 0.34 (right panel). (F) Survival of NOD/SCID mice xenotransplanted with hyperintense HCC cells transfected with Sh-Scr (n = 5) or Sh-HNF4A (n = 5).

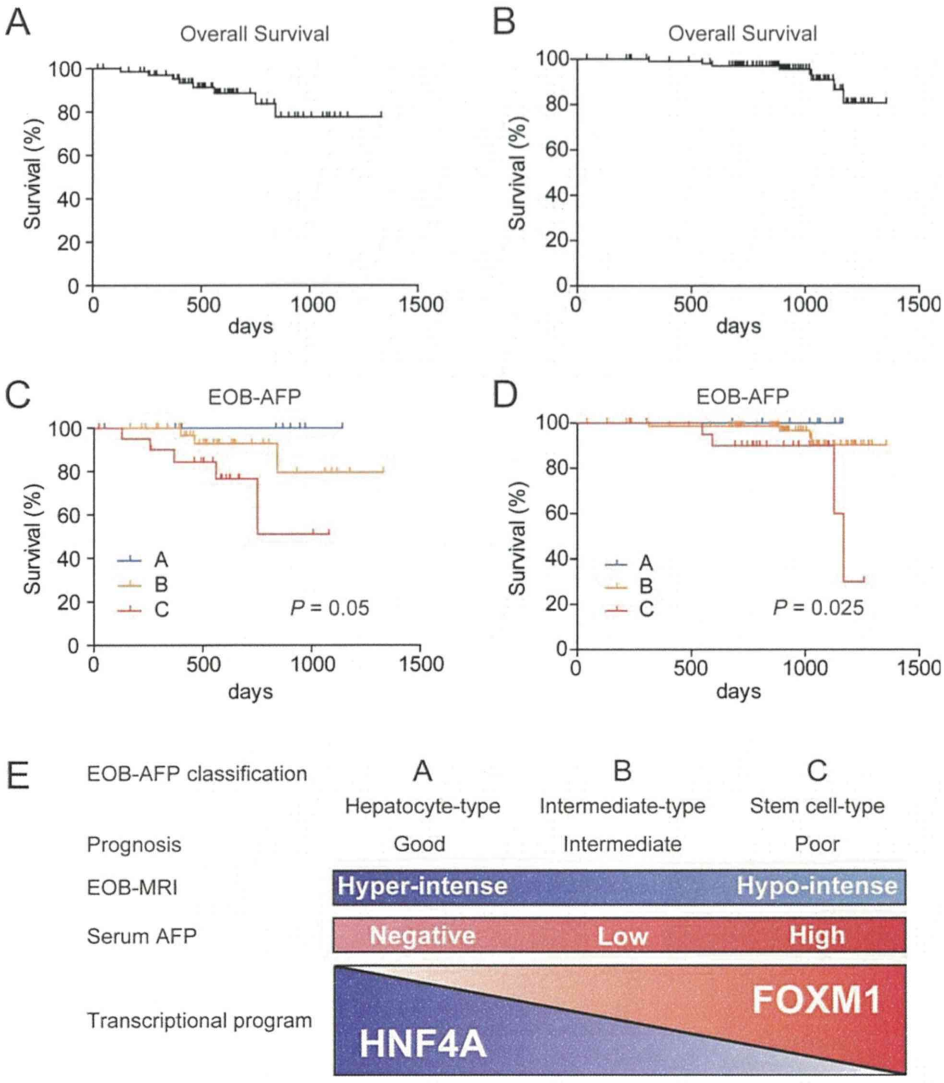

Fig. 4. Prognostic utility of the EOB-AFP classification. (A,B) Overall survival curves of Cohorts 1 (A) and 2 (B). (C,D) Overall survival curves of Cohorts 1 (C) and 2 (D) according to the EOB-AFP classification. (E) The EOB-AFP classification system and its molecular basis.

observed in Sh-HNF4A-transfected cells, whereas Sh-Scr-transfected cells still showed Gd-EOB-DTPA uptake with less tumorigenic capacity (Fig. 3E). Mice xenotransplanted with Sh-HNF4A-transfected cells had a worse prognosis compared with those xenotransplanted with Sh-Scr-transfected cells (Fig. 3F), indicating a crucial role for HNF4α in the maintenance of a mature hepatocyte-like, less aggressive HCC phenotype coupled with Gd-EOB-DTPA uptake capacity.

Prognosis of Early-Stage HCC by EOB-AFP Classification. Finally, we evaluated the prognosis of patients with HCC diagnosed by EOB-MRI and serum AFP. To exclude the potential effect of lead-time bias on survival analysis for HCCs at different stages, we evaluated the power of the EOB-AFP classification system to predict the prognosis of patients with early-stage BCLC stage 0 or A HCCs diagnosed by EOB-MRI in an independent multicenter cohort (Cohort 2). Nine of the 109 HCC cases (8.3%) were diagnosed with hyperintense HCCs and were found to be significantly associated with low serum AFP levels (Table 1). The clinicopathologic characteristics of the patients defined by the EOB-AFP classification are shown in Supporting Table 5. The median follow-up times in Cohorts 1 and 2 were 569 and 932 days, respectively. The 3-year overall survival rates in Cohorts 1 and 2 were 77.7% and 90.9%, respectively (Fig. 4A,B). The prognosis of HCC patients was not separated by TNM or BCLC stages because most of these patients were diagnosed at early stages (Fig. S4A-D); nevertheless, the EOB-AFP classification system robustly stratified HCCs according to survival with statistically significant differences between the classes (Fig. 4C,D). EOB-AFP class A patients had 100% overall survival, whereas class C patients had 30% overall survival at 1,200 days after radical resection in Cohort 2.